ORNL/TM-2022/2543

Preliminary Sensitivity Analysis for Sensors Impacts on Building Control Performance

Yanfei Li
Yeobeom Yoon
Yeonjin Bae
Piljae Im

October 2022

OAK RIDGE National Laboratory

ORNL IS MANAGED BY UT-BATTELLE LLC FOR THE US DEPARTMENT OF ENERGY

ORNL/TM-2022/2543

Electrification and Energy Infrastructures Division

PRELIMINARY SENSITIVITY ANALYSIS FOR SENSORS IMPACTS ON BUILDING CONTROL PERFORMANCE

Yanfei Li
Yeobeom Yoon
Yeonjin Bae
Piljae Im

October 2022

Prepared by
OAK RIDGE NATIONAL LABORATORY
Oak Ridge, TN 37831-6283
managed by
UT-BATTELLE LLC
for the
US DEPARTMENT OF ENERGY
under contract DE-AC05-00OR22725

CONTENTS

LIST OF FIGURES

LIST OF TABLES

EXECUTIVE SUMMARY

This report describes the preliminary sensitivity analysis for sensor impacts on building control performance through the US Department of Energy's Oak Ridge National Laboratory's two-story Flexible Research Platform building. The rooftop unit system provides cooling and heating to the building. The main heating coil is a gas heating coil. Each zone is served by a variable air volume box with an electricity reheat coil. The rooftop unit and variable air volume box controls adopted the practical control sequences from ASHRAE Guideline 36-2018: High-Performance Sequences of Operation. For sensors, the incipient (time-changing) sensor errors, including bias sensor error and precision sensor error, are the inputs of interest. The outputs are energy consumption and thermal comfort (e.g., the predicted percentage of dissatisfied occupants).

The large-scale simulation (3,600 cases) was conducted on a cloud platform by integrating sensor errors and ASHRAE Guideline 36 control sequences into an emulator based on the EnergyPlus simulation program with Python EMS. The surrogate models were developed based on cloud simulation results. The uncertainty analysis showed that the sensor errors substantially affect building energy consumption and thermal comfort. The sensitivity analysis shows a ranking of sensor error effects for each interested output item (e.g., cooling energy, reheat coil heating energy, predicted percentage of dissatisfied occupants).

In FY 2022, sensor locations, types, and costs were evaluated. Field testing in Oak Ridge National Laboratory's two-story Flexible Research Platform building regarding the effects of sensors was also performed. Finally, a comparative analysis was conducted based on the field test results and emulator results.

1. INTRODUCTION

Sensors are critical components for controls in buildings. Sensors collect desired information for input to controls for subsequent control actions. In the past 10 years, the focus has been on advanced controls, and sensors were not well studied. When sensors work in unhealthy or faulty conditions, the control benefits are reduced regardless of the effectiveness of the controls (Bae et al. 2021). For buildings, multiple components directly influence the sensor placement and deployment, such as sensor errors, sensor locations, sensor types, and sensor costs.

This study systematically investigated the effects of sensor errors on building controls and building performance. Two aspects define sensor errors: bias error and precision (random) error. Limited studies have been conducted on fixed sensor errors, and no studies have investigated incipient errors. To investigate these errors, a multiple-step workflow was proposed to create a complete framework. The framework comprises (1) physics-based emulator development with sensor errors and control sequences, (2) large-scale simulations for sensor error samplings to the controls on the cloud, (3) surrogate model development based on cloud simulation results for sensitivity analysis, and (4) sensitivity analysis and uncertainty analysis for the sensors and desired outputs (e.g., energy consumption, thermal comfort). This framework is extensible and scalable to other sensor components, such as sensor locations, types, and costs. The details of each step are discussed in the following sections.

2. SENSOR EFFECTS AND EVALUATION FRAMEWORK

The framework for the impacts and evaluation of sensors comprises multiple components: a physics-based emulator with control and sensor modules, cloud simulation, surrogate model generation, uncertainty analysis, and sensitivity analysis. The overall workflow is illustrated in Figure 1.

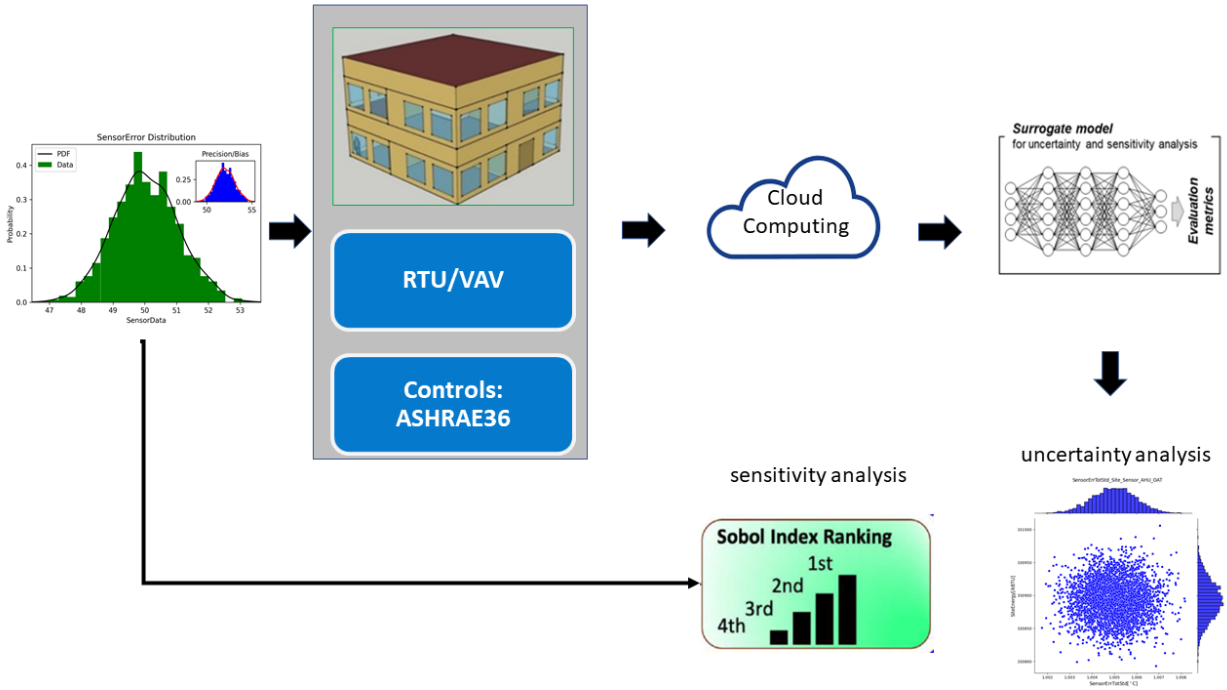

Figure 1. Sensor impact and evaluation framework. (RTU: rooftop unit; VAV: variable air volume)

2.1 SENSOR SETS

Based on extensive literature reviews, 34 sensors were identified. They are typical sensors used to operate rooftop unit (RTU) and variable air volume (VAV) systems in small to medium office buildings. The sensors were prioritized based on the severity of indoor air (IA) temperature impacts, which can significantly affect energy efficiency and occupant thermal comfort.

The identified sensors are frequently used in commercial buildings. They are listed in Table 1.

Table 1. Comprehensive sensor list

Location	Measurement	Priority	Location	Measurement	Priority
Room	IA temperature	1	RTU	OA CO_2	4
Room	IA humidity	3	RTU	OA flow rate	3
Room	IA CO_2	4	RTU	SA temperature	1
Room	Lighting condition	5	RTU	SA humidity	3
Room	Occupancy	5	RTU	SA CO_2	4
VAV box	SA temperature	1	RTU	SA flow rate	3
VAV box	SA humidity	3	RTU	RA temperature	2
VAV box	SA flow rate	1	RTU	RA humidity	3

Location	Measurement	Priority	Location	Measurement	Priority
Main duct	Static pressure	2	RTU	RA CO_2	4
Exhaust fan	EA temperature	4	RTU	RA flow rate	3
Exhaust fan	EA humidity	4	RTU	MA temperature	2
Exhaust fan	EA flow rate	4	RTU	MA humidity	3
Exhaust fan	EA CO_2	4	RTU	MA CO_2	4
Other	Plug load	5	RTU	MA flow rate	3
Other	Lighting load	5	RTU	Refrigerant temperature	5
RTU	OA temperature	1	RTU	Refrigerant pressure	5
RTU	OA humidity	3	RTU	Refrigerant flow rate	5

SA = supply air; EA = exhaust air; OA = outdoor air; RA = return air; MA = mixing air

Based on the actual HVAC system configuration of Oak Ridge National Laboratory's two-story Flexible Research Platform (FRP-2) building, five sensor types were selected for the following reasons: (1) the IA temperature is the most important variable to be controlled to meet the heating and cooling set point temperatures, (2) the VAV box supply air (SA) temperature and SA flow rate directly impact the IA temperature from the control perspective, (3) RTU system-level operation also directly impacts the VAV box operations, and (4) RTU outdoor air (OA) temperature and SA temperature are important for determining the system-level energy consumption. The sensor types are listed in Table 2.

Table 2. Selected sensor list

Location	Measurement	Priority	Note
Room	IA temperature	1	IA temperature
VAV box	SA temperature	1	VAV box SA temperature
VAV box	SA flow rate	1	VAV box SA flow rate
RTU	OA temperature	1	OA temperature
RTU	SA temperature	1	SA temperature

2.2 SENSOR ERRORS (INPUTS)

The total sensor error comprises two components: bias error and precision (random) error. For a sensor, an ideal reading (or true reading) exists at a given time step, as shown by the black line in Figure 2. The bias error is the system deviation from the ideal readings, as shown by the green dotted line in Figure 2. The precision error is the random deviation from the average sensor readings, as shown by the blue lines in Figure 2. The horizontal axis represents the time. The vertical axis represents any variable we need to get from sensor readings.

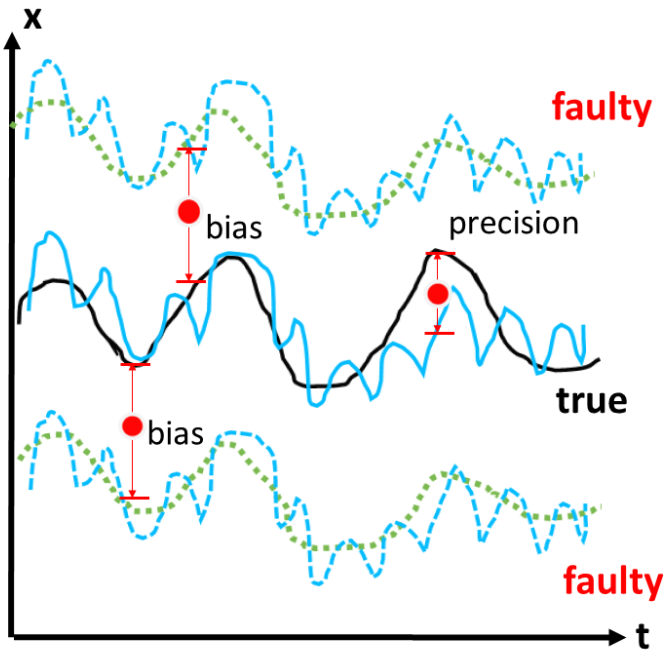

Figure 2. Sensor error diagram.

For this study, the incipient error was incorporated into the sensors for control studies. This error follows normal distributions. Figure 3 illustrates the normal distribution of bias error, precision error, and total error. This figure just shows the elements of sensor errors. The numbers in the plots are for demonstration purposes, not representing the actual sensor errors.

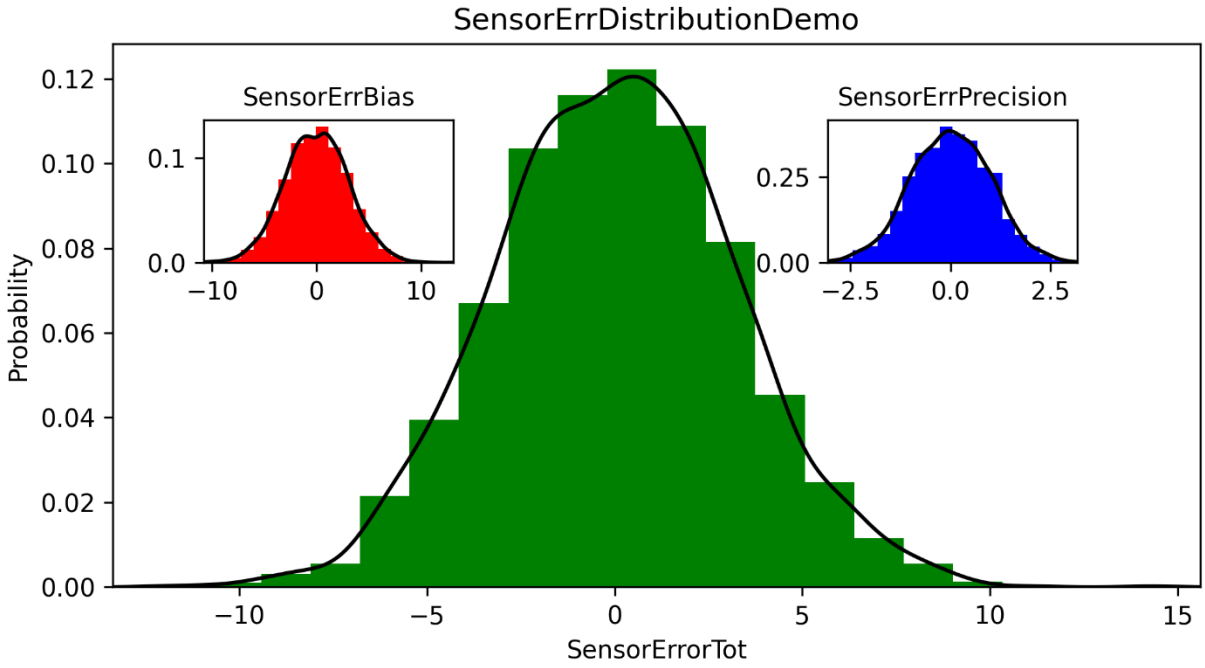

Figure 3. Sensor error sampling distributions.

Equations (1)–(3) describe the sensor errors:

$$Error_{bias} = normal_{distribution}(0, \sigma_{bias}), \quad (1)$$

$$Error_{precision} = normal_{distribution}(0, \sigma_{precision}), \text{ and} \quad (2)$$

$$Sensor_{readings} = Sensor_{idealreadings} + Error_{bias} + Error_{precision}, \quad (3)$$

where σ_{bias} is the standard deviation of bias error, and $\sigma_{precision}$ is the standard deviation of precision error.

The sensor errors were incorporated based on the emulator of EnergyPlus and Python EMS. Because of the technical difficulties from larger airflow sensor errors, the airflow sensor errors need to be within an effective range. The standard deviations for the five types of selected sensors are shown in Table 3.

Table 3. Standard deviation of selected sensor errors

Location	Measurement	Standard deviation	Precision
Room	IA temperature (°C)	1	0.1
VAV box	SA temperature (°C)	1	0.1
VAV box	SA flow rate (m^3/s)	0.005	0.0005
RTU	OA temperature (°C)	1	0.1
RTU	SA temperature (°C)	1	0.1

2.3 ASHRAE GUIDELINE 36 CONTROL LOGIC FOR RTU AND SINGLE-DUCT VAV SYSTEMS

The installed HVAC systems to the FRP-2 building are the RTU, in which the cooling is from a direct expansion cooling coil, and heating is from the gas heating coil. The FRP-2 building has 10 conditioned zones. Each conditioned zone is served by each VAV box with an electricity reheat coil. The air handling unit (AHU) connects all the zone VAV boxes and the RTU. Control logic from ASHRAE Guideline 36-2018: High-Performance Sequences of Operation (ASHRAE Guideline 36) was developed for the RTU and VAV box.

2.3.1 AHU: Trim and respond set point logic

The first control logic is the trim and respond (T&R) set point logic for the AHU. T&R logic resets set points of the pressure, temperature, or other variables in the AHU or plant side. T&R logic reduces the set point at a fixed rate until the zone thermal comfort is no longer satisfied, and then it generates the request. The set point is increased in response to a sufficient number of requests. By adjusting the importance of each zone's requests, the critical zones will always be satisfied. If there is not a sufficient number of requests, then the set point decreases at a fixed rate.

The term *request* refers to a request to reset a static pressure or temperature set point generated by downstream zones or AHUs. These requests are sent upstream to the AHU or plant that supplies the zone or area that generated the request. Figure 4 shows an example of the T&R control provided by ASHRAE Guideline 36.

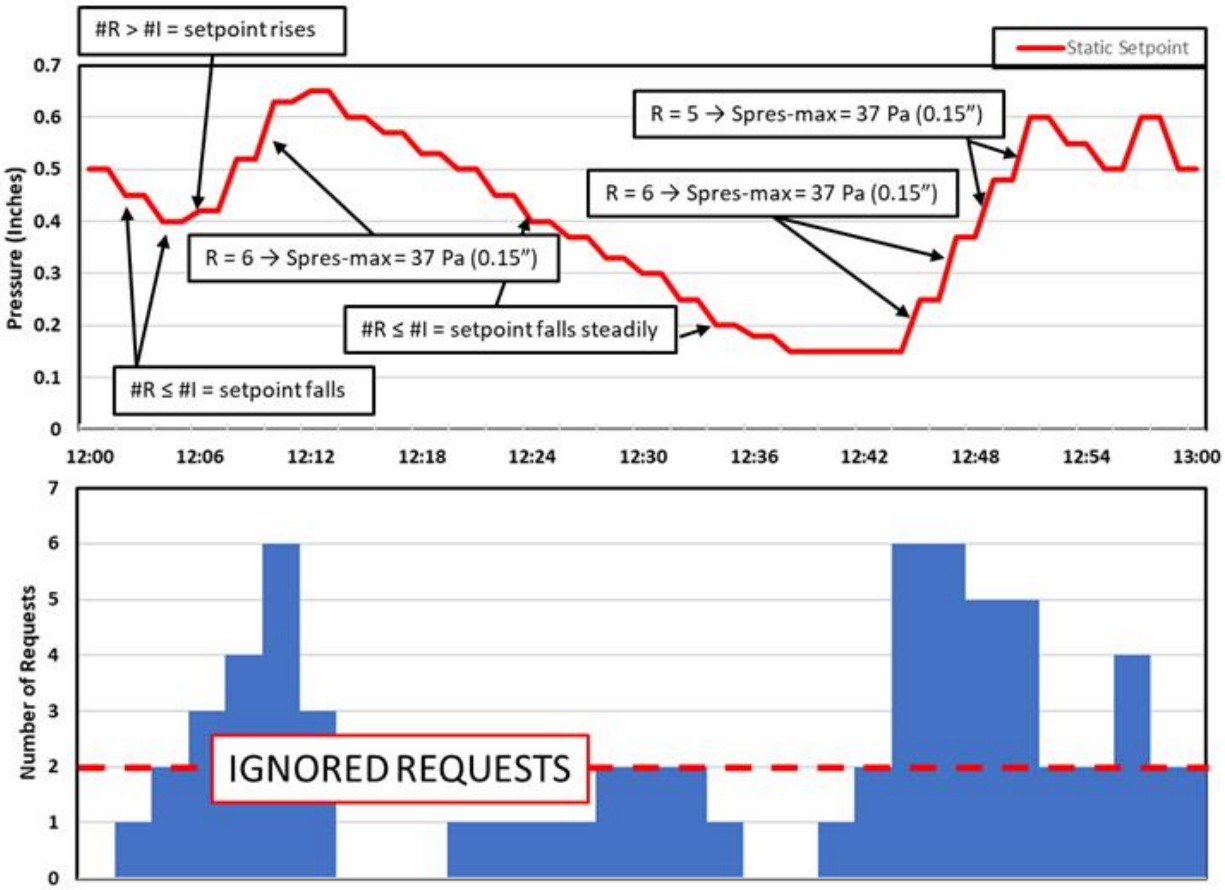

Figure 4. Example of the T&R control logic from ASHRAE Guideline 36 (ASHRAE, n.d.; Taylor 2015).

T&R control was used to reset the RTU SA set point temperature in the emulator. When the OA temperature was higher than the maximum OA temperature (21°C [69.8°F]), the RTU SA temperature was set to the minimum RTU SA set point temperature (12°C [53.6°F]). When the OA temperature was lower than the minimum OA temperature (16°C [60.8°F]), the RTU SA temperature was set to the maximum RTU SA set point temperature (18°C [64.4°F]). If the OA temperature was between the minimum and maximum OA temperature when the OA temperature was increased, the RTU SA temperature was increased linearly from the minimum RTU SA set point temperature to the maximum RTU SA set point temperature. For T&R control, as ASHRAE Guideline 36 describes, fewer than two requests were ignored.

2.3.2 VAV box control logic

The VAV box control is the second control logic applied to the emulator. Figure 5 shows the control logic for the VAV box from ASHRAE Guideline 36. The control logic has three sections, which correspond to the heating season, cooling season, and deadband. The control logic uses the heating loop demand concept. Heating loop demand is the ratio (as a percentage) of the actual required heating load of the VAV box to the size of the VAV box. Equation (4) describes how to calculate the heating loop demand:

$$Heating\ loop\ demand = \frac{Heating\ load\ of\ the\ VAV\ box}{Capacity\ of\ the\ VAV\ box} \times 100\%. \quad (4)$$

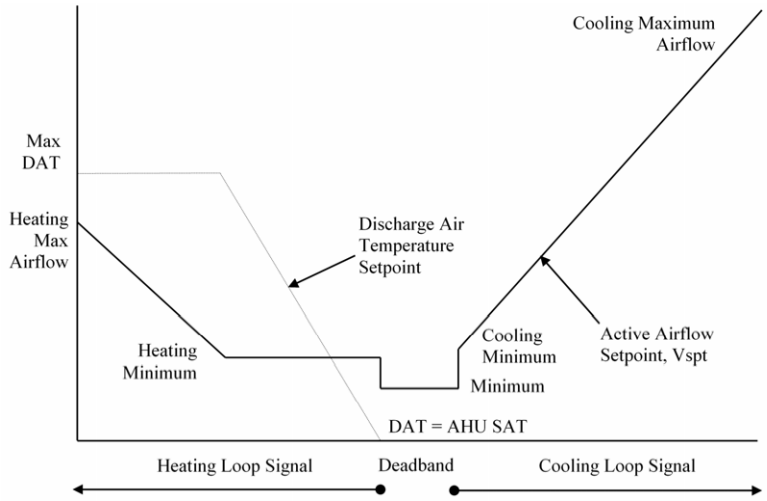

Figure 5. Control logic for VAV box from ASHRAE Guideline 36 (ASHRAE, n.d.; Taylor 2015).

The detailed logics are threefold:

- In the heating season, when the heating loop is less than or equal to 50%, the discharge air (DA) set point temperature of the VAV box is increased from the RTU SA temperature to the maximum DA set point temperature of the VAV box, and the minimum SA flow rate is maintained. When the heating loop is greater than 50%, if the DA temperature of the VAV box is greater than IA temperature plus 3°C (5°F), then the SA flow rate of the VAV box is increased from the minimum SA flow rate to the maximum SA flow rate while maintaining the maximum DA set point temperature of the VAV box.
- In the cooling season, the DA temperature of the VAV box is the same as the RTU SA temperature because no option exists to decrease the SA temperature using the VAV box. Therefore, VAV box control is linked with T&R control in the cooling season, when the VAV box control must be considered the RTU SA temperature. The four cooling SA set point temperature reset requests are as follows:
  - If the IA temperature exceeds the indoor cooling set point temperature by 3°C (5°F) for 2 min after the suppression period resulting from an RTU SA set point temperature change via the T&R control, then send three requests.
  - If the IA temperature exceeds the indoor cooling set point temperature by 2°C (3°F) for 2 min after the suppression period resulting from an RTU SA set point temperature change via the T&R control, then send two requests.
  - If the cooling loop is greater than 95%, then send one request until the cooling loop is less than 85%.
  - If the cooling loop is less than 95%, then send no request.

  In terms of the SA flow rate in the cooling season, the SA flow rate of the VAV box is increased from the minimum SA flow rate to the maximum SA flow rate as the cooling loop is increased.
- In the deadband, when neither heating nor cooling are needed, the SA flow rate is set to the minimum SA flow rate, and the DA temperature of the VAV box is set to the RTU SA temperature.

2.4 LARGE-SCALE SIMULATION

The large-scale simulation was based on a commercial cloud platform, Microsoft Azure. In total, 3,600 cases were simulated on the cloud. The inputs were the sensor errors incorporated into the five selected sensors for the FRP-2 building emulator, as described in Table 2. The sensor errors were obtained using

normal distribution samplings. EnergyPlus internal programming limits caused simulation crashes when larger sensor errors were incorporated. The standard deviations of sensor errors were based on multiple trials. The thresholds were based on engineering experience, domain knowledge, and actual sensor readings. The outputs were the target variables for energy consumption and thermal comfort, such as fan electricity consumption and reheat coil electricity energy in the VAV box.

The basic diagram is shown in Figure 6. The basic workflow is as follows:

1. A Python script was developed to generate 3,600 simulation input data files. Each input data file was associated with a Python class of sensor errors through Python EMS. During the simulation, at each time step, a new sensor error (including bias and precision) was injected into the ideal sensor readings from EnergyPlus.

2. After 3,600 cases were generated, they were uploaded to the Azure cloud platform.

3. In the Azure cloud platform, a bash script selected the appropriate virtual machine configurations (e.g., memory and hard drive, as shown in Table 4) and a number of virtual machines. The team's subscription included 300 nodes (virtual machines).

4. The Azure cloud provided a job scheduler, which automatically distributed all 3,600 cases across 300 nodes.

5. The simulation ran automatically until all cases were accomplished.

6. Finally, all the results were selected to set up the data sets (inputs and outputs) to create the black box models.

The configuration for the cloud is shown in Table 4.

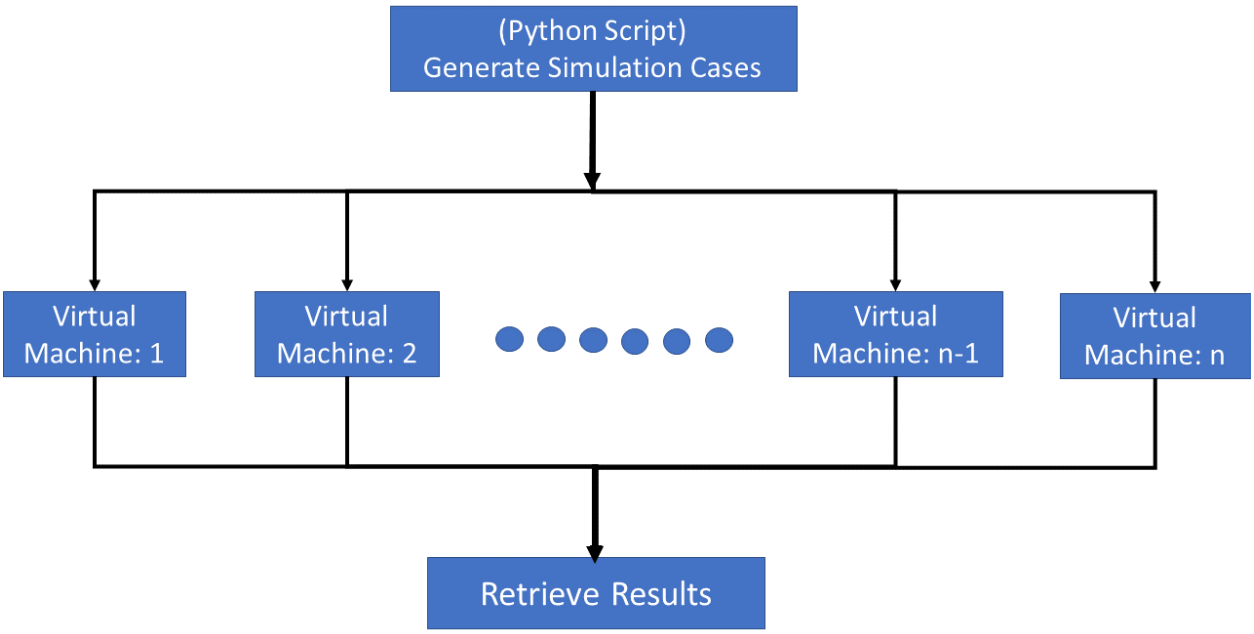

Figure 6. Cloud simulation workflow.

Table 4. Cloud configurations

Machine type	Cores/node	Memory/node	Storage/ node	Total nodes	Time executed
Standard_D16d_v4	16	64 GB	600 GB	300	9 h

The sensor errors were sampled using a normal distribution for each time step. The sensor readings from EnergyPlus used the sensor errors to form the faulty or hacked sensor readings. The hacked sensor readings were used as inputs to control sequences to calculate new set points. These new set points were used to control the performance of buildings. Ultimately, the simulated energy consumption and thermal comfort were different from the results obtained using the ideal sensor readings.

3. SURROGATE MODEL

To accomplish sensitivity analysis, the surrogate model was developed based on cloud simulations. The long short-term memory (LSTM) model was selected because it includes previous time step input impacts. These impacts are important because inertia phenomena exist in buildings. The LSTM model internally reflects the thermal inertia.

3.1 PRINCIPLE

The LSTM model is a neural network model suitable for time series forecasting. For building energy simulations, the results are time series variables. The thermal state of buildings at previous time steps has certain impacts on the later time steps. The main purpose of the LSTM model is to find the mapping of inputs and outputs. Figure 7 shows that the input variables were transformed into multiple routes as a way of including previous states' impacts. The detailed mathematics are not included here because the goal was to use the LSTM model to make a black box model.

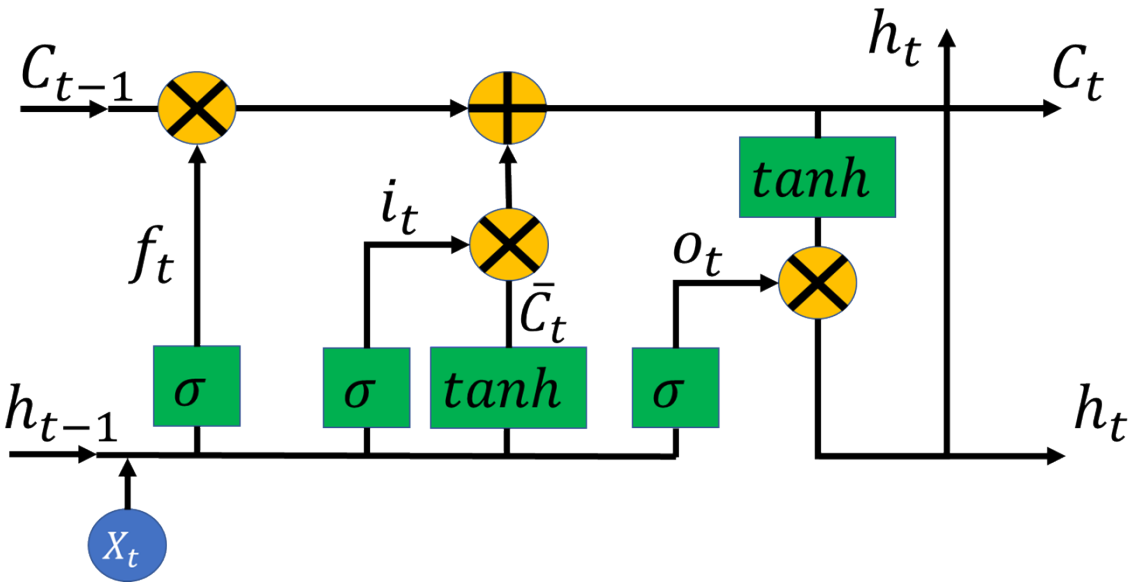

Figure 7. LSTM cell structure.

3.2 TRAINING AND TESTING

The whole data set was divided into a training data set (80% of total) and a validation data set (20% of total). The training data set was used to learn the weights of input variables to output variables. The validation data set was used to test the accuracy of the surrogate model prediction from the emulator output variables. The data sets were shuffled to avoid the input data internal impacts. The root mean square error was used to quantify the modeling accuracy:

$$RMSE = \sqrt{\frac{\Sigma_1^N (y_i - \hat{y}_i)^2}{N}}, \tag{5}$$

where $RMSE$ is the root mean square error, y_i is the emulator output variable, $\hat{y}_i$ is the surrogate model output variable, and N is the total number of variables in the prediction.

3.3 INPUT VARIABLES AND OUTPUT VARIABLES

The surrogate model established the mapping relationship between input and output variables. The input variables were based on the FRP-2 EnergyPlus models. A detailed list of variables is provided in Table 5.

Table 5. Input variables

Variable name	Quantity	Unit
OAT (OA temperature)	1	°C
OA relative humidity	1	%
OA pressure	1	Pa
Wind speed	1	m/s
Wind direction	1	°
Horizontal infrared radiation rate	1	w/m^2
Diffuse solar radiation rate	1	w/m^2
Direct solar radiation rate	1	w/m^2
Lighting energy	1	w/m^2
Internal heat gains: equipment	1	w/m2
People activity	1	1
Sensor bias: AHU OAT	1	°C
Sensor precision: AHU OAT	1	°C
Sensor total error: AHU OAT	1	°C
Sensor bias: AHU SAT (SA temperature)	1	°C
Sensor precision: AHU SAT	1	°C
Sensor total error: AHU SAT	1	°C
Sensor bias: zone VAV SAF (supply airflow)	10	kg/s
Sensor precision: zone VAV SAF	10	kg/s
Sensor total error: zone VAV SAF	10	kg/s
Sensor bias: zone VAV SAT	10	°C
Sensor precision: zone VAV SAT	10	°C
Sensor total error: zone VAV SAT	10	°C
Sensor bias: zone air temperature	10	°C
Sensor precision: zone air temperature	10	°C
Sensor total error: zone air temperature	10	°C
Total	**107**	

The output variables were also based on FRP-2 EnergyPlus simulation models. A detailed list of output variables is provided in Table 6.

Table 6. Output variables

Variable	Quantity	Unit
Fan electricity rate	1	W
Main cooling coil sensible cooling rate	1	W
Main cooling coil electricity rate	1	W
Main heating coil heating rate	1	W
Zone air sensible heating rate	10	W
Zone air sensible cooling rate	10	W
Zone air temperature	10	°C
Zone predicted percentage dissatisfied	10	%
VAV box reheat energy	10	J
Total	**54**	

3.4 WORKFLOW FOR SURROGATE MODEL TRAINING

In total, 3,600 simulation cases were simulated on the cloud. Each case generated 1.3 GB of data with 1 min time resolution. A 4.7 TB data set was obtained. To expedite the surrogate model training, a distributed framework was used. The workflow is shown in Figure 8. Through the cloud, 100 32-core machines were used. The 3,600 cases were divided into 20 groups, or cores, with each group responsible for 180 cases. After all training was completed at each group, the final model parameters were obtained by averaging model parameters from the 20 groups of training.

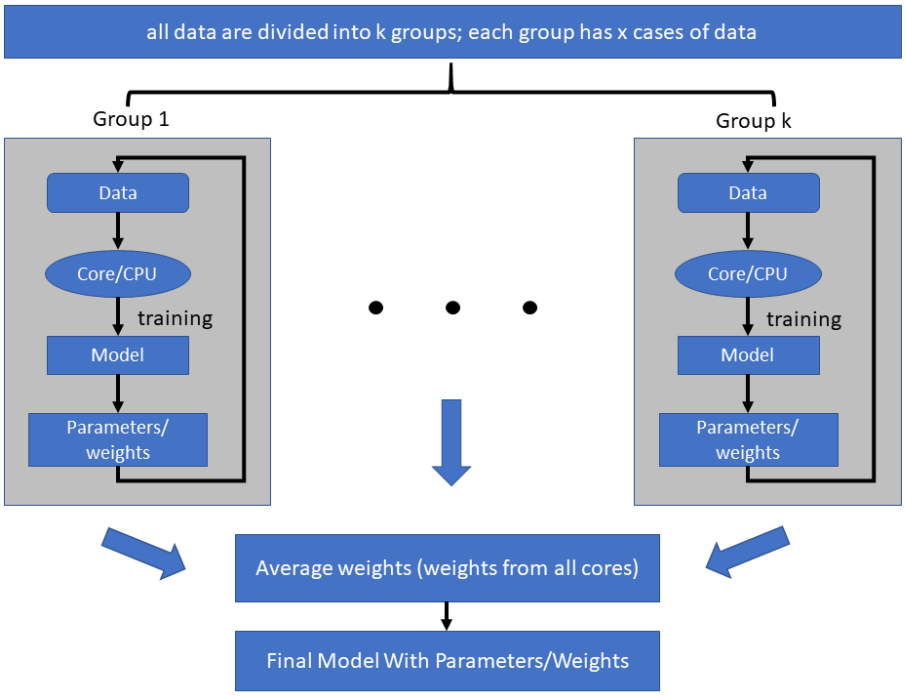

Figure 8. Distributed training of surrogate models.

4. UNCERTAINTY ANALYSIS

4.1 PRINCIPLE

Uncertainty analysis assesses the uncertainty of output/target variables in the model in which the inputs are under uncertainty samplings. The purpose of this uncertainty analysis is to identify how output variables distributed in response to uncertainties of input values. Generally, wider distribution of output variables corresponds to increased sensitivity of the output variables to the input variables. For this uncertainty analysis, the large-scale simulation (3,600 cases) was conducted on a cloud platform. Figure 9 illustrates the overall process of the uncertainty analysis. The standard deviations of input values (sensor errors) of the uncertainty analysis are listed in Table 5, and selected output variables are listed in Table 6. Before the uncertainty analysis, HVAC system controls based on the ASHRAE Guideline 36 were applied using the Python EMS function, as described in Section 2.3. Input values for the system control were obtained from the simulation results. Then, the total sensor error (total error = bias error + precision error) was added to the HVAC system control. Using the physics-based emulator, 3,600 cases were generated. The results are described in Section 4.2.

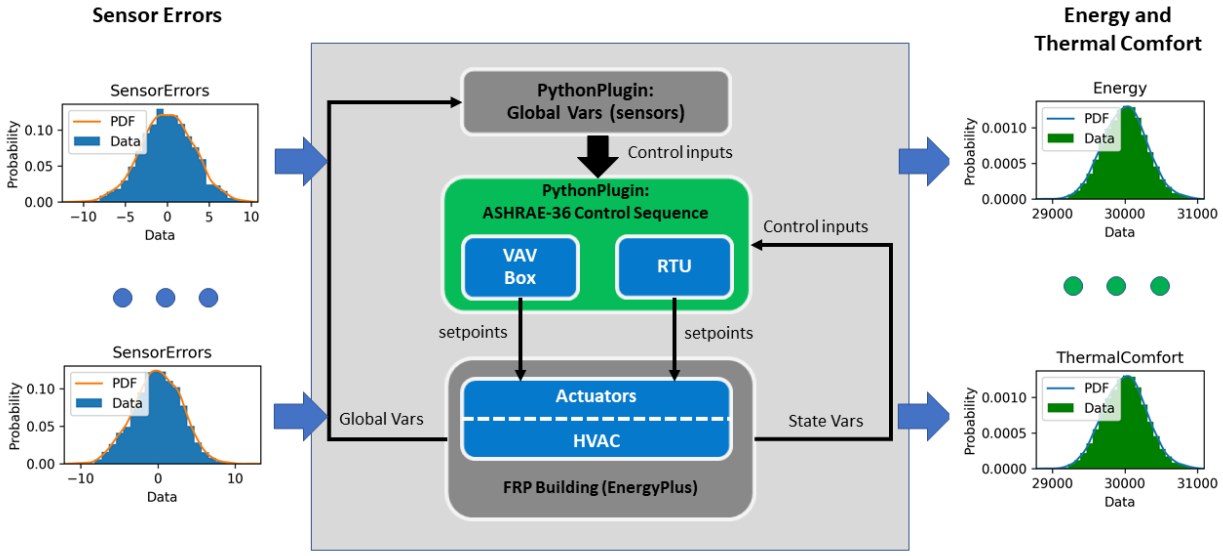

Figure 9. Uncertainty analysis process. PDF = probability distribution function.

4.2 UNCERTAINTY ANALYSIS

For large-scale simulations, each case generates the aggregated energy consumption: site energy, heating energy, cooling energy, and fan energy. The baseline results are 304,083 kBtu for site energy, 60,081 kBtu for heating energy, 105,482 kBtu for cooling energy, and 50,422 kBtu for fan energy. Figure 10 shows the energy distributions and baseline energy items. It shows that the energy consumption is much higher than in the baseline cases. Half red dot denotes the baseline energy items.

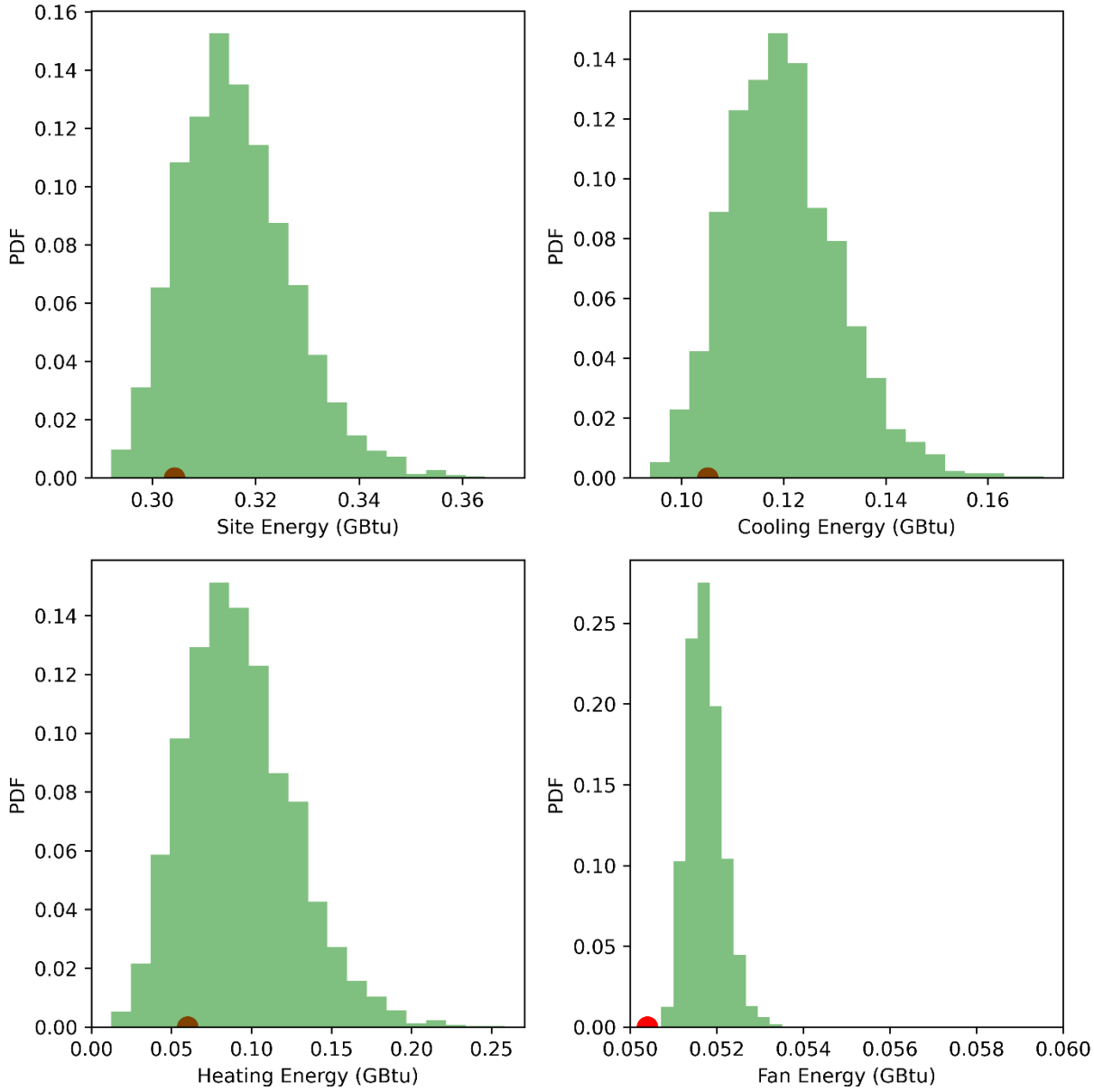

Figure 10. Energy distributions and baseline energy items. PDF = probability distribution function.

Figure 11 shows the site energy consumption with averaged sensor error distributions. The top left graph shows the AHU OA temperature (OAT) and SA temperature (SAT) sensor errors for the site energy consumption. The top right graph shows the VAV box SAT temperature sensor errors and site energy consumption. The bottom left graph shows the zone temperature sensor errors with site energy consumption. The bottom right graph shows the VAV box supply airflow (SAF) sensor errors with site energy consumption. The distributed data show normal distributions instead of a linear relationship. The site energy consumption was approximately 334,000–346,000 kBtu/year based on the distribution of total sensor errors. The variation of total site energy consumption was 12,000 kBtu/year, which is 3.5% of the average site energy consumption (340,083 kBtu/year).

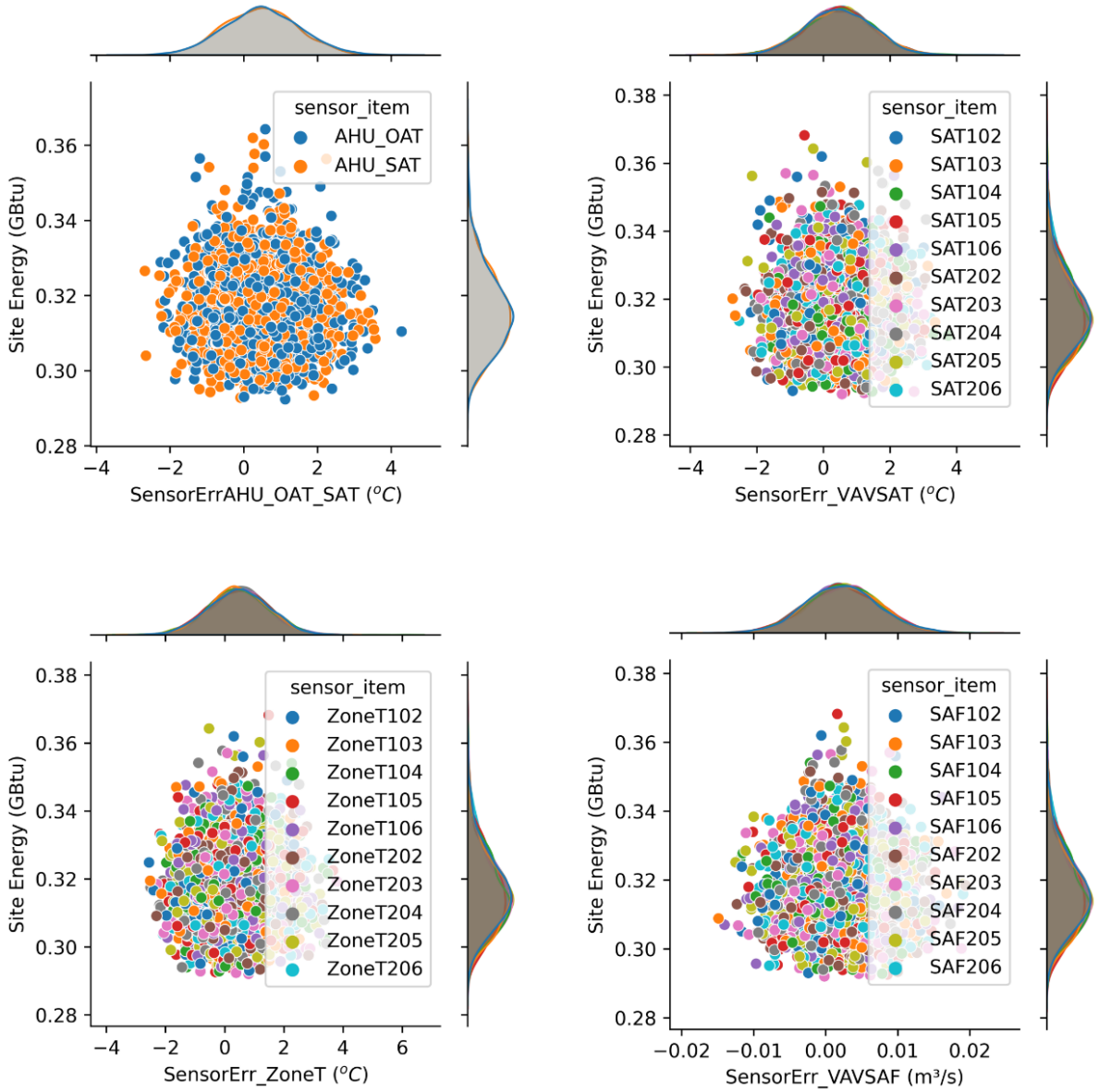

Figure 11. Site energy and sensor errors.

Figure 12 shows the total heat energy consumption with averaged sensor error distributions. The top left graph shows the AHU OAT and SAT sensor errors for heating energy consumption. The top right graph shows the VAV box SAT temperature sensor errors for heating energy consumption. The bottom left graph shows the zone temperature sensor errors for heating energy consumption. The bottom right graph shows the VAV box SAF sensor errors for heating energy consumption. The distributed data show normal distributions instead of a linear relationship. The heating energy consumption was approximately 20,130–26,400 kBtu/year based on the distribution of total sensor errors. The variation of total site energy consumption was 1,045 kBtu/year, which is 4.5% of the average site energy consumption (23,265 kBtu/year).

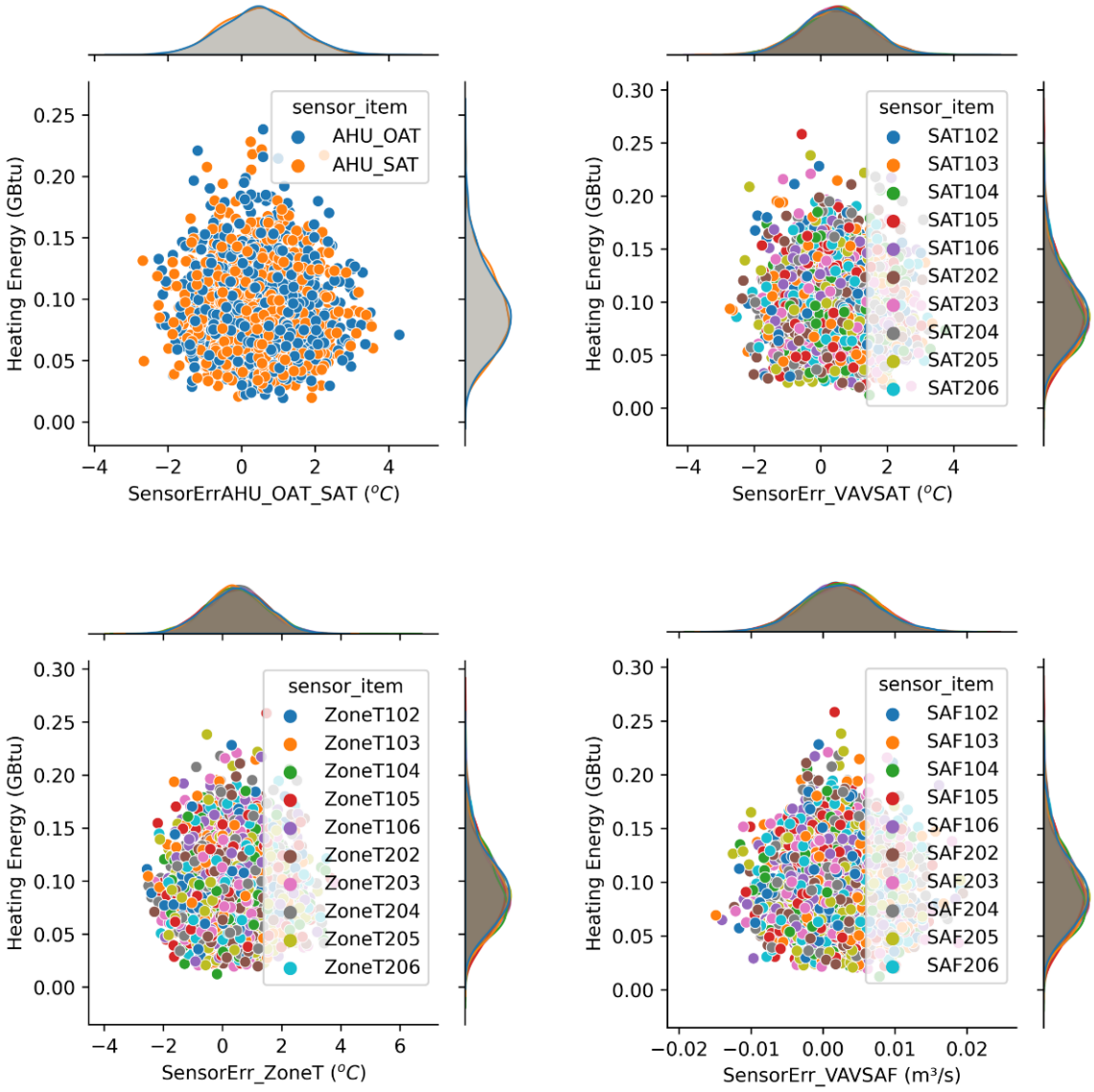

Figure 12. Heating energy and sensor errors.

Figure 13 shows the total cooling energy consumption with averaged sensor error distributions. The top left graph shows the AHU OAT and SAT sensor errors for cooling energy consumption. The top right graph shows the VAV box SAT temperature sensor errors for cooling energy consumption. The bottom left graph shows the zone temperature sensor errors for cooling energy consumption. The bottom right graph shows the VAV box SAF sensor errors for cooling energy consumption. The distributed data show normal distributions instead of a linear relationship. The cooling energy consumption was approximately 93,320–174,000 kBtu/year based on the distribution of total sensor errors. The variation of total site energy consumption was 13,446 kBtu/year, which is 10.5% of the average site energy consumption (133,660 kBtu/year).

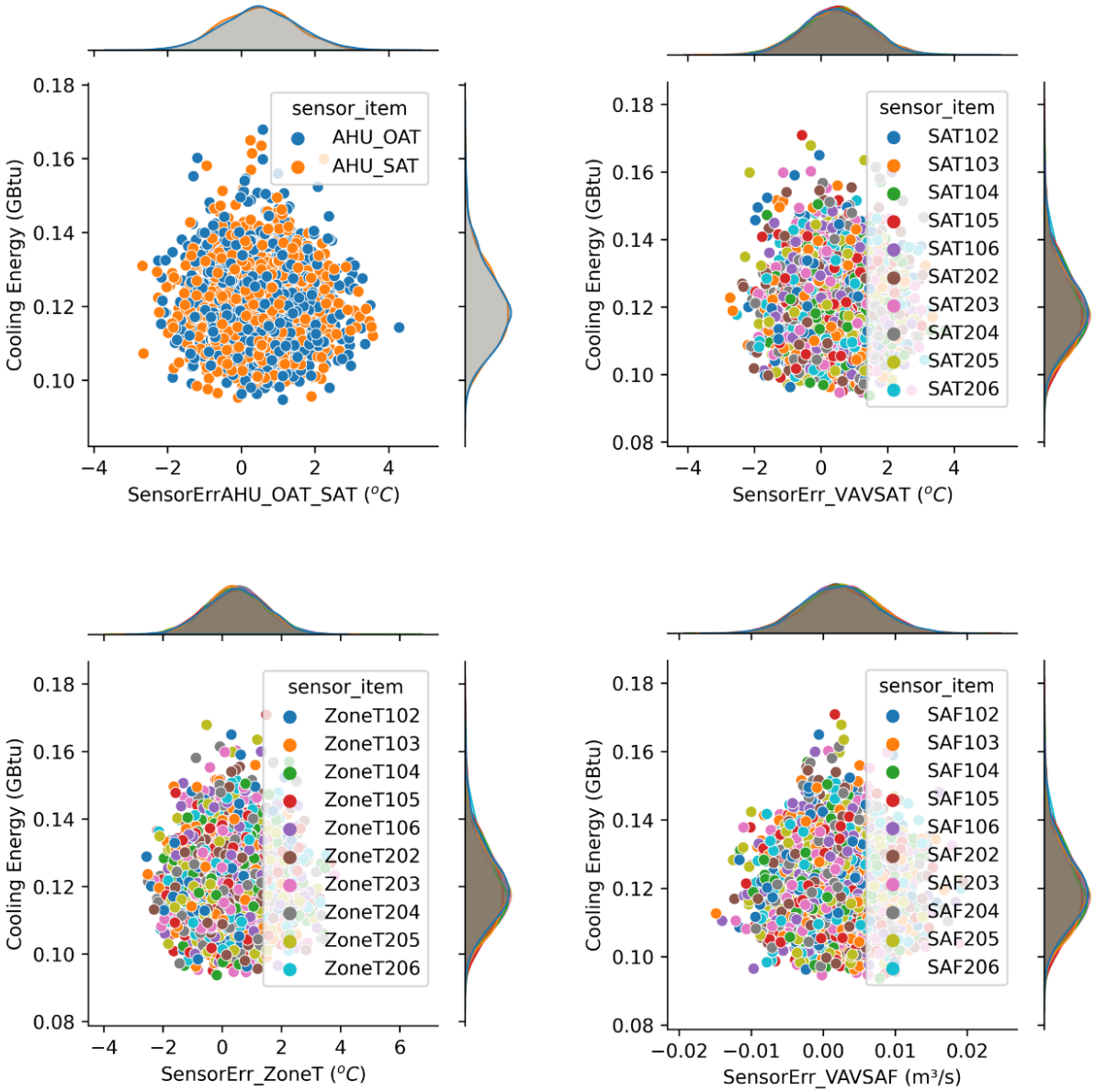

Figure 13. Cooling energy and sensor errors.

Figure 14 shows the total fan energy consumption with averaged sensor error distributions. The top left graph shows the AHU OAT and SAT sensor errors for fan energy consumption. The top right graph shows the VAV box SAT temperature sensor errors for fan energy consumption. The bottom left graph shows the zone temperature sensor errors for fan energy consumption. The bottom right graph shows the VAV box SAF sensor errors for fan energy consumption. The distributed data show normal distributions instead of a linear relationship. The fan energy consumption was approximately 50,501–53,900 kBtu/year based on the distribution of total sensor errors. The variation of total site energy consumption was 567 kBtu/year, which is 1.1% of the average site energy consumption (52,200 kBtu/year).

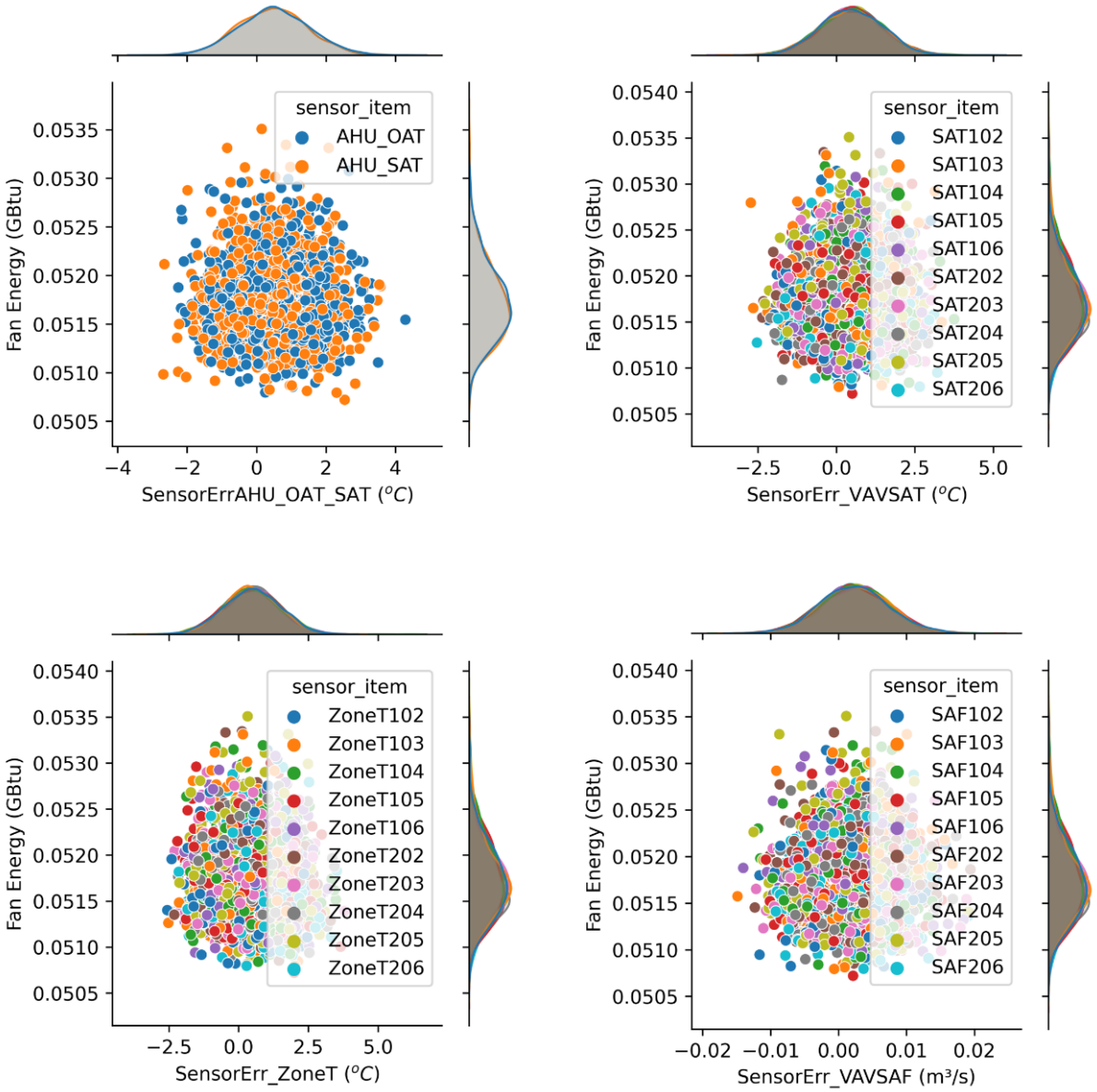

Figure 14. Fan energy and sensor errors.

5. SENSITIVITY ANALYSIS

5.1 PRINCIPLE

The sensitivity analysis identified which sensor errors have stronger effects on energy consumption and thermal comfort. A ranking of sensor error effects was obtained using sensitivity analysis index values. Sensitivity analysis can be performed in various ways, such as local and global approaches (Tian 2013; Pang et al. 2020). Different methods have certain advantages and drawbacks. As a preliminary exploration, this project applied the Sobol (Tian 2013) method to calculate the sensitivity index.

The principle is described as

$$Y = f_0 + \sum_{i=1}^{d} f_i(X_i) + \sum_{i<j}^{d} f_{ij}(X_i,X_j) + \cdots + f_{1,2,\ldots,d}(X_1,X_2,\ldots,X_d), \quad (4)$$

where Y is one of the interested model outputs, X_i is the model input with uncertainty, d is the total number of model inputs with uncertainties, f_0 is the constant, f_i is the function of X_i, and f_{ij} is the function of X_i and X_j.

The sensitivity index S_i is given as

$$S_i = \frac{V_i}{Var(Y)}, \quad (5)$$

where V_i is the variance with respect to variable input X_i, and $Var(Y)$ is the total variance of the output variable Y.

The definitions of these variances are

$$V_i = Var_{X_i}(E_{X_{\sim i}}(Y|X_i)), \quad (6)$$

$$Var(Y) = \sum_{i=1}^{d} V_i + \sum_{i<j}^{d} V_{ij} + \ldots + V_{12\ldots d}, \quad (7)$$

where $\sim i$ indicates all the input variables except X_i.

Note that

$$\sum_{i=1}^{d} S_i + \sum_{i<j}^{d} S_{ij} + \ldots + S_{12\ldots d} = 1. \quad (8)$$

The workflow for sensitivity analysis is shown in Figure 15.

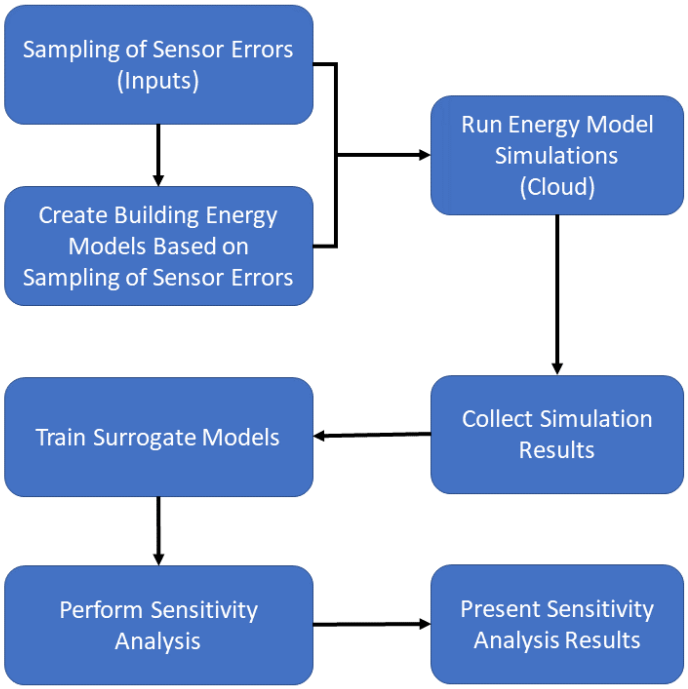

Figure 15. Sensitivity analysis flowchart.

5.2 SENSITIVITY ANALYSIS RESULTS

Based on the simulation results, AHU-level and zone-level sensitivity analyses were performed. The results are presented in the following subsections. For zone-level analysis, there are two floors, and each floor has five zones. They have similar patterns regarding the sensitivity analysis. One zone from each floor (zone 102 and zone 204) was selected to demonstrate the sensitivity analysis.

5.2.1 System SA analysis

The AHU power consumption was studied. Figure 16 illustrates the sensitivity index for cooling power. The cooling power is sensitive to the random errors of the SAT sensors and OAT sensors, total errors of the SAT sensors and OAT sensors, and bias errors of the SAT sensors and OAT sensors. They have equal impacts on the cooling power demands.

Figure 17 illustrates the sensitivity index for fan power demands. The sensor impacts are similar to the cooling power.

Figure 18 illustrates the sensitivity index for main heating coil heating rates. The SAT and OAT sensors are the most dominant sensors.

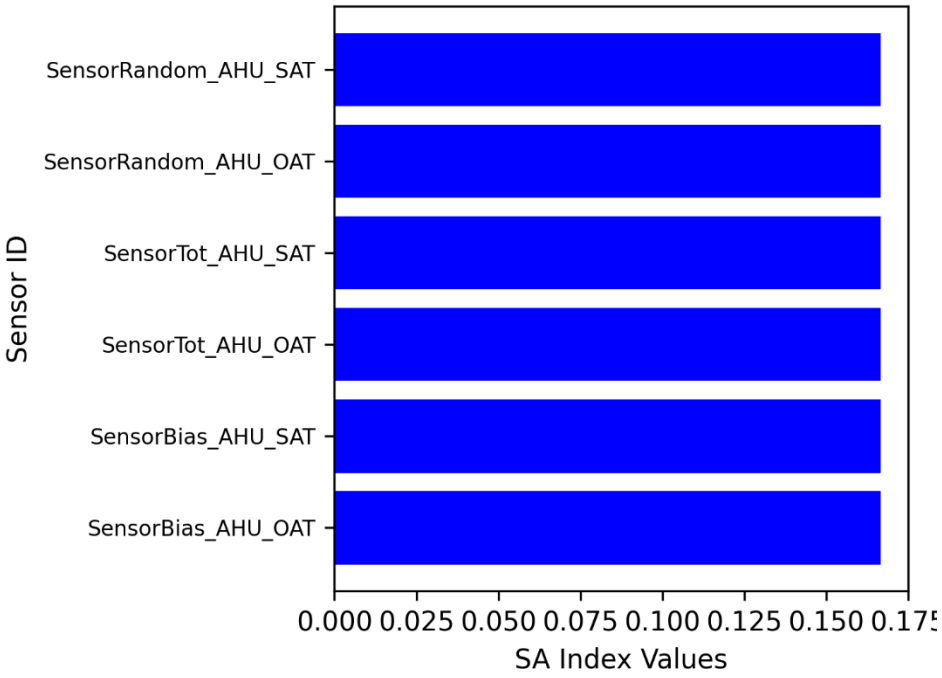

Figure 16. SA for RTU cooling power.

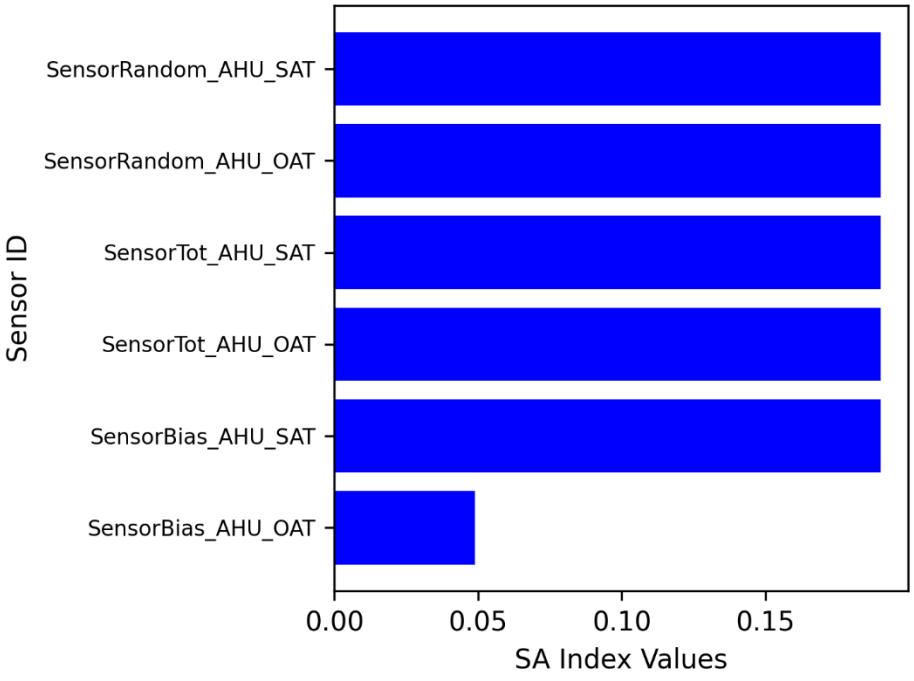

Figure 17. SA for RTU fan power.

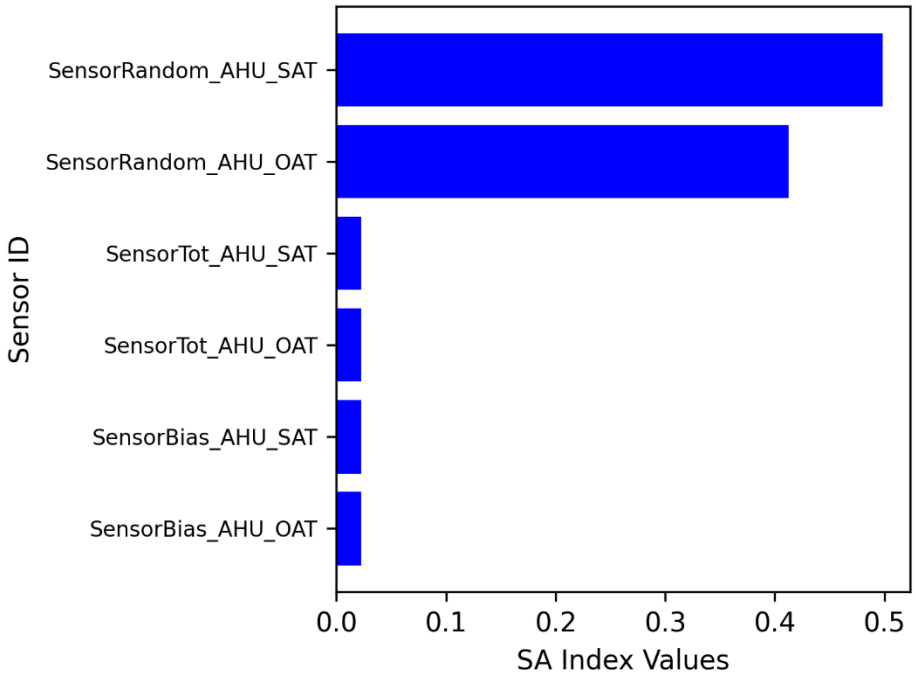

Figure 18. SA for RTU main heating coil heating rate.

5.2.2 Zone 204 SA analysis

At the zone level, four energy consumption variables (zone temperature, zone sensible heating, zone sensible cooling, and reheat coil energy consumption) and one thermal comfort variable (zone predicted percentage of dissatisfied occupants [PPD]) were selected. Figure 19 shows the ranking of sensitivity indices for zone air temperature. Overall, the system- and zone-level sensors impacted the zone temperature. The sensor with the highest sensitivity index was the zone air temperature sensor with random error. The random errors are the most influential, followed by total errors, and then bias errors. Figure 20 shows the ranking of sensitivity indices for zone sensible heating. The zone air temperature sensor with random error has the highest sensitivity index. Figure 21 shows the zone sensible cooling effects from the sensors. Figure 22 shows the effects on reheat coil energy. Figure 23 shows the sensitive index ranking for zone thermal comfort (PPD). Across zone 204 output items, the random errors consistently had stronger effects.

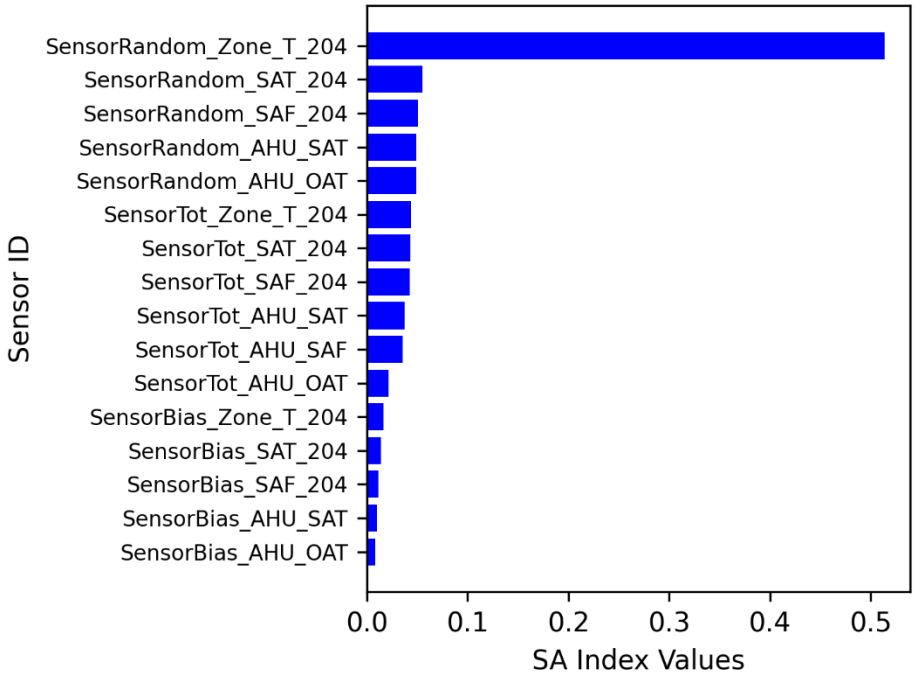

Figure 19. SA for zone 204 air temperature.

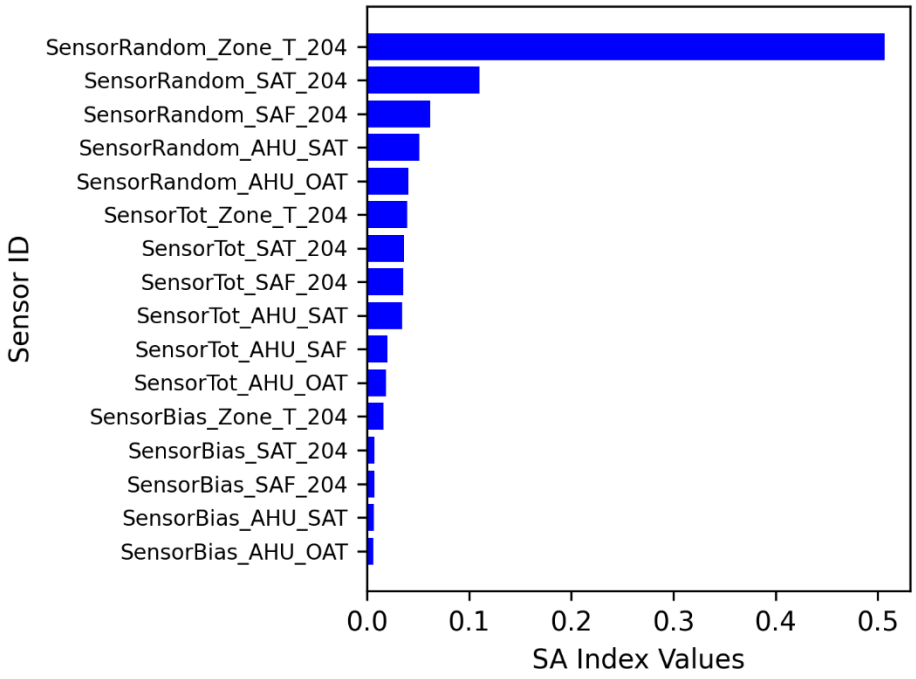

Figure 20. SA for zone 204 sensible heating.

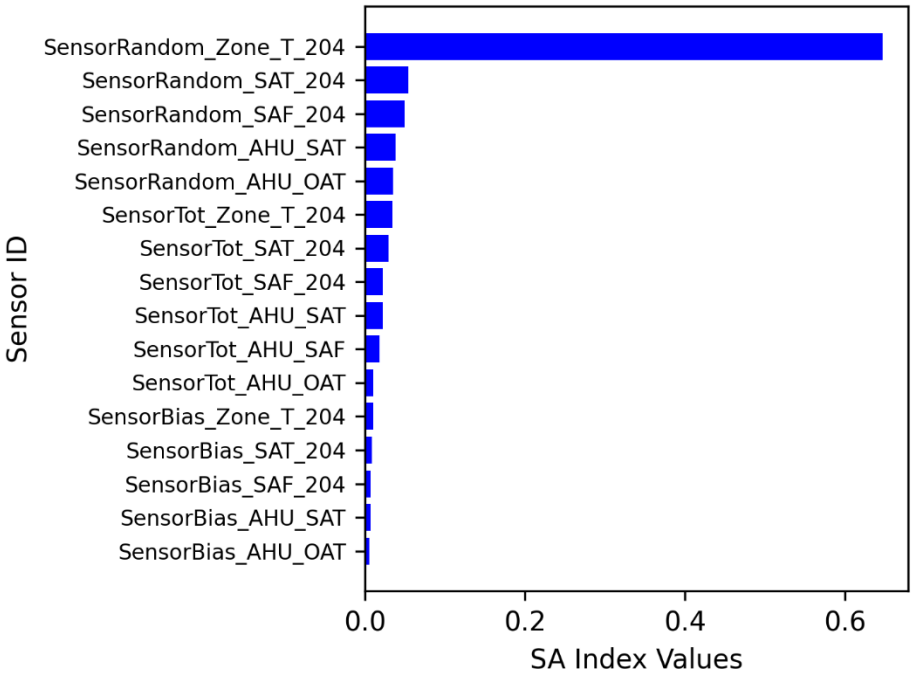

Figure 21. SA for zone 204 sensible cooling.

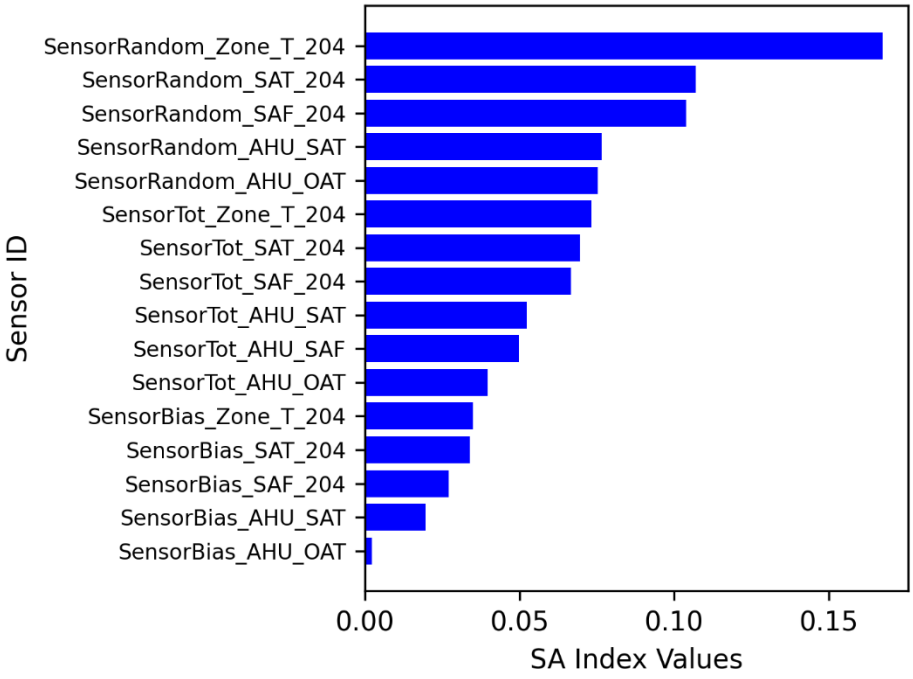

Figure 22. SA for zone 204 reheat coil energy.

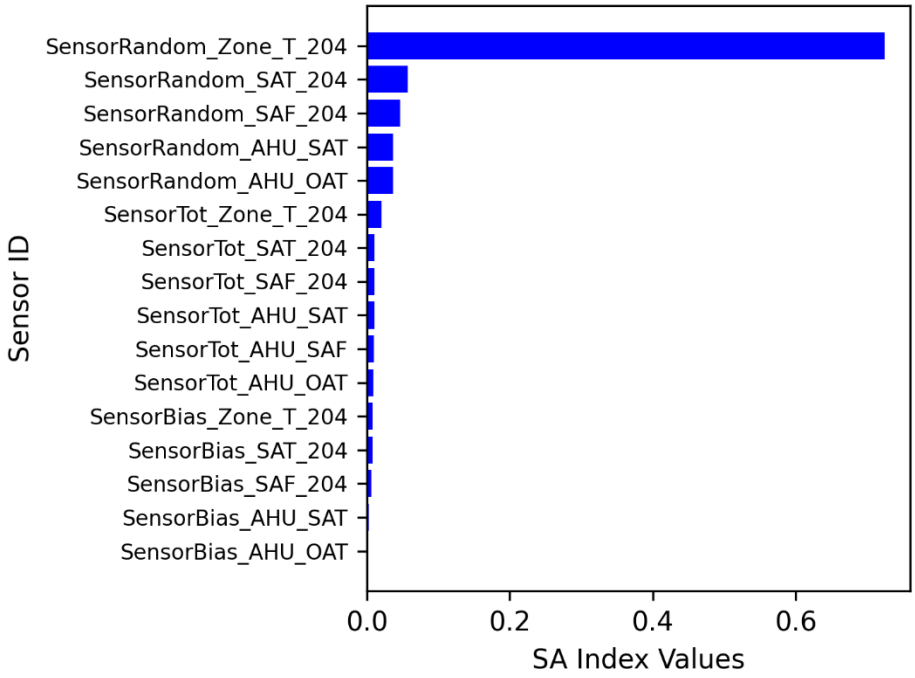

Figure 23. SA for zone 204 PPD.

5.2.3 Zone 102 SA analysis

Sensitivity analysis for zone 102 was performed similarly to that of zone 204. The effects of sensor errors on four energy consumption variables (zone temperature, zone sensible heating, zone sensible cooling, and reheat coil energy consumption) and one thermal comfort item (zone PPD) were analyzed. Figure 24 shows the ranking of sensitivity indices for zone 102 air temperature. The system- and zone-level sensors affected the zone temperature. The zone air temperature sensor with random error had the highest sensitivity index. Figure 25 shows the ranking of sensitivity indices for zone sensible heating. The zone air temperature sensor with random error had the highest sensitivity index. Figure 26 shows the zone sensible cooling effects from the sensors. Figure 27 shows the effects on reheat coil energy. Figure 28 shows the sensitivity index ranking for zone thermal comfort (PPD). Across zone 102 output variables, random errors consistently had stronger effects.

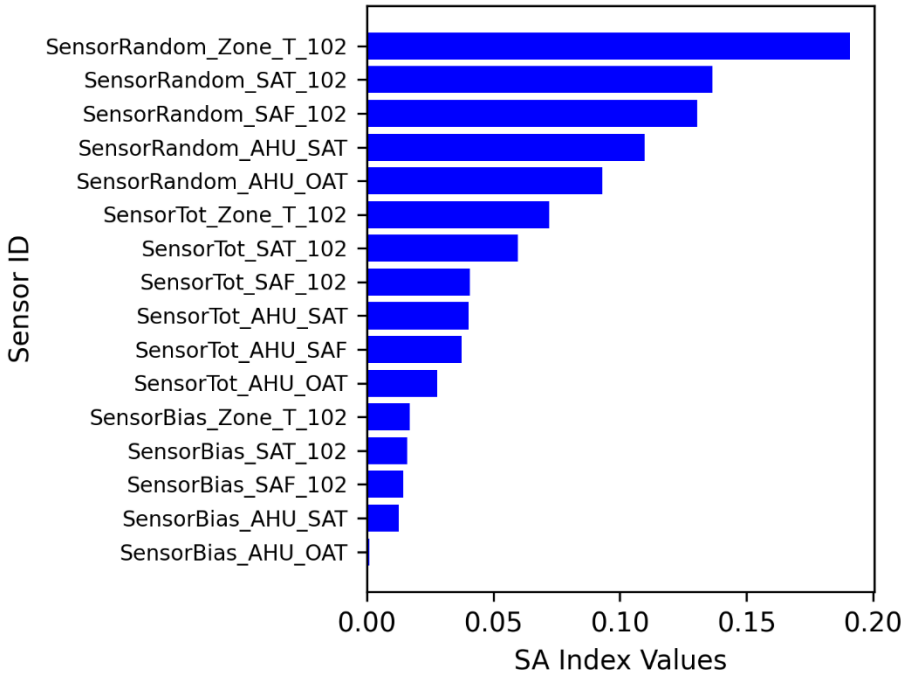

Figure 24. SA for zone 102 air temperature.

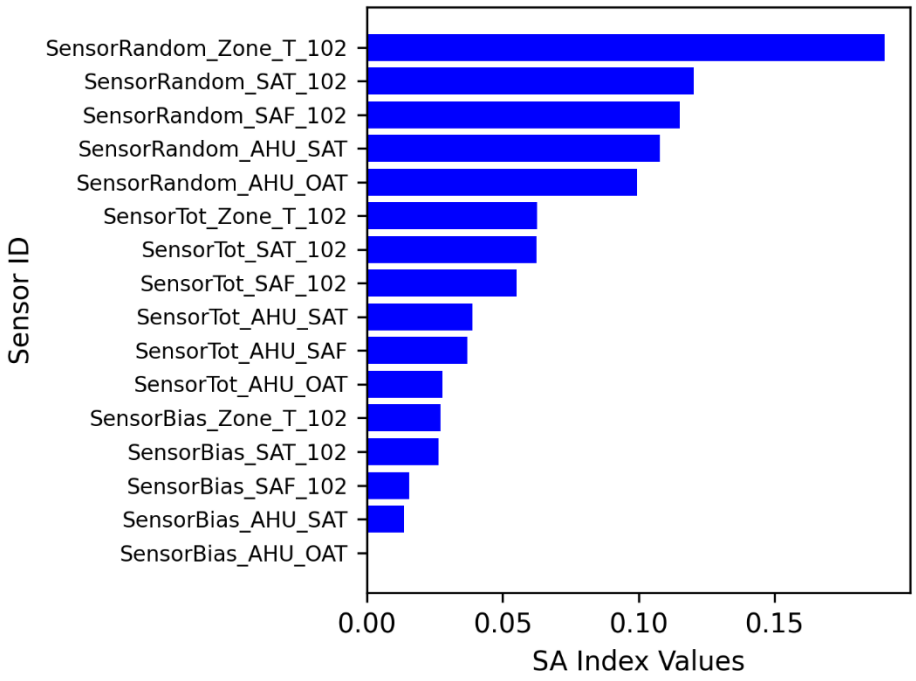

Figure 25. SA for zone 102 sensible heating energy.

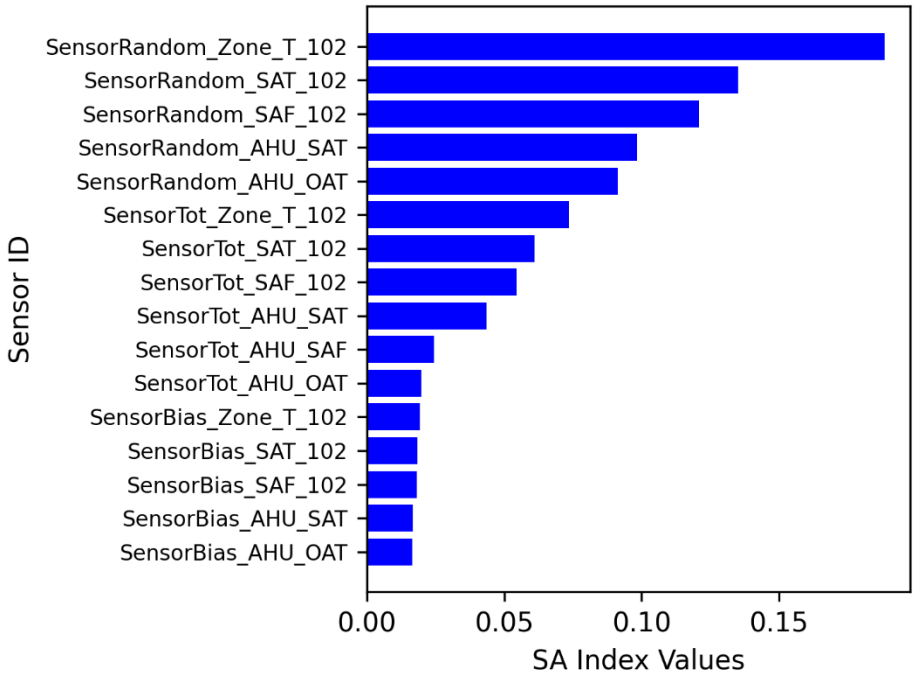

Figure 26. SA for zone 102 sensible cooling energy.

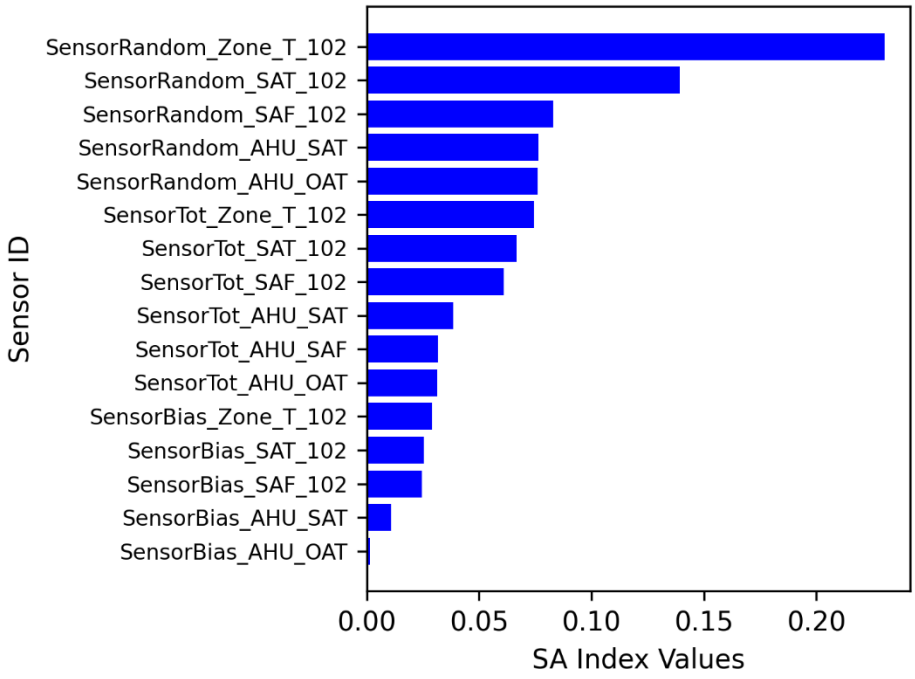

Figure 27. SA for zone 102 reheat coil energy.

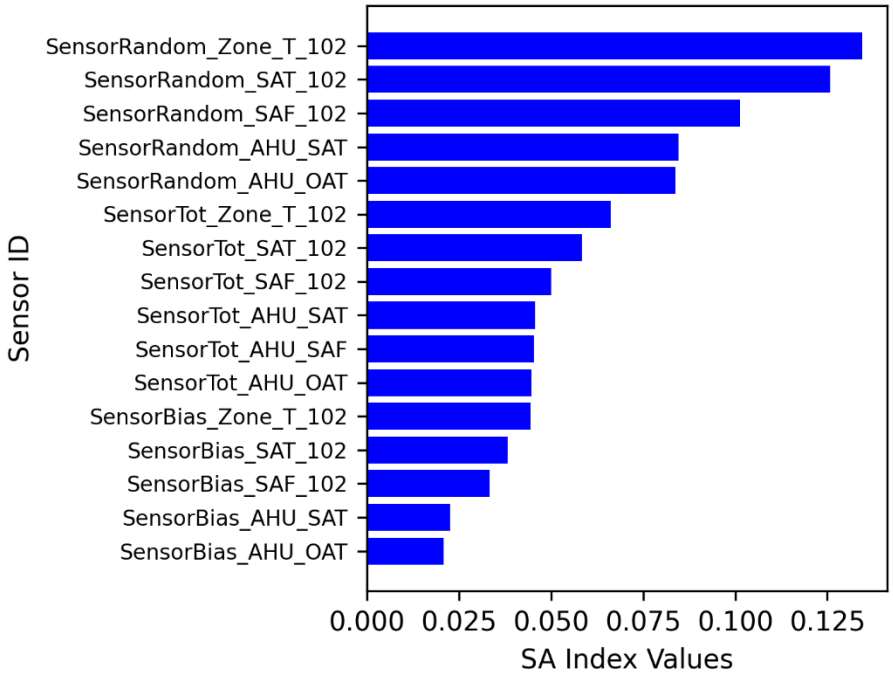

Figure 28. SA for zone 102 PPD.

6. CONCLUSIONS

This study investigated the preliminary sensitivity analysis for energy consumption and thermal comfort with respect to sensor errors. The sensor errors had two components: bias error and precision (random) error. The sensor samplings were distributed with normal distributions.

The energy consumption was classified into system levels (cooling capacity and power demands) and zone levels (zone air temperature, zone sensible heating, zone sensible cooling, and zone reheat coil energy). The thermal comfort (PPD) at the zone level was also investigated.

The cloud simulations were conducted based on the sensor samplings and 3,600 simulation cases. The results were collected to train surrogate models for sensitivity analysis.

The uncertainty and sensitivity analyses were conducted with respect to sensor errors and energy/thermal comfort variables. The uncertainty analysis showed that the sensor errors and energy consumptions have a nonlinear relationship. The energy consumptions had wide distributions compared with the baseline model with sensor error uncertainties.

The sensitivity analysis was performed at system and zone levels. At the system level, the random errors for SA and OA temperature sensors had the most significant effects. At the zone level, the random errors are the most influential, followed by total errors, and then bias errors.

In the future, other sensitivity analysis methods will be explored for comparative analysis, and other surrogate models might be explored.

7. REFERENCES

ASHRAE. 2018. “ASHRAE Guideline 36-2018: High-Performance Sequences of Operation.” ASHRAE.

Bae, Yeonjin, Saptarshi Bhattacharya, Borui Cui, Seungjae Lee, Yanfei Li, Liang Zhang, Piljae Im, et al. 2021. “Sensor Impacts on Building and HVAC Controls: A Critical Review for Building Energy Performance.” *Advances in Applied Energy* 4 (November): 100068. https://doi.org/10.1016/j.adapen.2021.100068.

Pang, Zhihong, Zheng O’Neill, Yanfei Li, and Fuxin Niu. 2020. “The Role of Sensitivity Analysis in the Building Performance Analysis: A Critical Review.” *Energy and Buildings* 209 (February): 109659. https://doi.org/10.1016/j.enbuild.2019.109659.

Taylor, Steven. 2015. “Resetting Setpoints Using Trim & Respond Logic.” *Ashrae Journal* 11: 52–57.

Tian, Wei. 2013. “A Review of Sensitivity Analysis Methods in Building Energy Analysis.” *Renewable and Sustainable Energy Reviews* 20: 411–19.